Slip-Stacked Perylenediimides as an Alternative Strategy for High Efficiency Nonfullerene Acceptors in Organic Photovoltaics
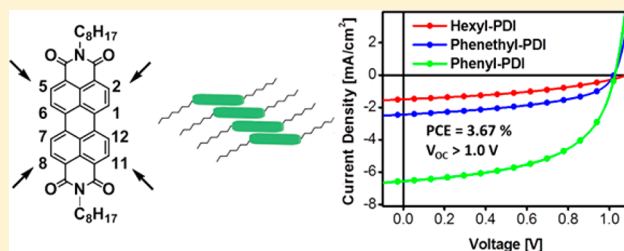
Patrick E. Hartnett,[†,∥] Amod Timalsina,[†,∥] H. S. S. Ramakrishna Matte,[†,‡,∥] Nanjia Zhou,[‡] Xugang Guo,[†] Wei Zhao,[§] Antonio Facchetti,[†,§] Robert P. H. Chang,*[‡] Mark C. Hersam,*[†,‡] Michael R. Wasielewski,*[†] and Tobin J. Marks*[†,‡]

[†]Department of Chemistry and the Materials Research Center, and [‡]Department of Materials Science and Engineering and the Materials Research Center, The Argonne-Northwestern Solar Energy Research Center, Northwestern University, 2145 Sheridan Road, Evanston, Illinois 60208, United States

[§]Polyera Corporation, 8045 Lamon Avenue, Skokie, Illinois 60077, United States

Ⓢ *Supporting Information*

ABSTRACT: Perylenediimide (PDI)-based acceptors offer a potential replacement for fullerenes in bulk-heterojunction (BHJ) organic photovoltaic cells (OPVs). The most promising efforts have focused on creating twisted PDI dimers to disrupt aggregation and thereby suppress excimer formation. Here, we present an alternative strategy for developing high-performance OPVs based on PDI acceptors that promote slip-stacking in the solid state, thus preventing the coupling necessary for rapid excimer formation. This packing structure is accomplished by substitution at the PDI 2,5,8,11-positions ("headland positions"). Using this design principle, three PDI acceptors, N,N-bis(n-octyl)-2,5,8,11-tetra(n-hexyl)-PDI (**Hexyl-PDI**), N,N-bis(n-octyl)-2,5,8,11-tetraphenethyl-PDI (**Phenethyl-PDI**), and N,N-bis(n-octyl)-2,5,8,11-tetraphenyl-PDI (**Phenyl-PDI**), were synthesized, and their molecular and electronic structures were characterized. They were then blended with the donor polymer **PBTI3T**, and inverted OPVs of the structure ITO/ZnO/Active Layer/MoO$_3$/Ag were fabricated and characterized. Of these, 1:1 **PBTI3T:Phenyl-PDI** proved to have the best performance with J_{sc} = 6.56 mA/cm^2, V_{oc} = 1.024 V, FF = 54.59%, and power conversion efficiency (PCE) = 3.67%. Devices fabricated with **Phenethyl-PDI** and **Hexyl-PDI** have significantly lower performance. The thin film morphology and the electronic and photophysical properties of the three materials are examined, and although all three materials undergo efficient charge separation, **PBTI3T:Phenyl-PDI** is found to have the deepest LUMO, intermediate crystallinity, and the most well-mixed domains. This minimizes geminate recombination in **Phenyl-PDI** OPVs and affords the highest PCE. Thus, slip-stacked PDI strategies represent a promising approach to fullerene replacements in BHJ OPVs.

INTRODUCTION

In recent years, the field of organic photovoltaics (OPVs) has been an area of intense research because these devices offer a potentially efficient, cost-effective, and scalable approach for solar energy conversion.[1−4] Although OPV efficiencies have been rapidly increasing, with multiple reports of power conversion efficiencies (PCE) exceeding 10%, they still lag behind typical inorganic solar cells.[5,6] Nevertheless, OPVs can be mass produced using solution based roll-to-roll processing from inexpensive, earth-abundant, and environmentally benign materials. Therefore, OPVs offer the potential to eclipse inorganic solar cells in cost per watt and eventually achieve grid-parity. The vast majority of efficient OPV systems are based on bulk-heterojunctions (BHJs) of either small molecule or polymer donors mixed with fullerene-based acceptors to form interpenetrating networks of electron and hole conducting pathways.[7−10] Fullerenes have many unique charge carrier capabilities, and these have been exploited in well-optimized systems to obtain internal quantum efficiencies approaching

100% and fill factors approaching 80%.[11−14] However, despite successes in laboratory scale devices, fullerenes are not an ideal material for production on an industrial scale. They are expensive to synthesize, difficult to modify chemically, and are unstable in air.[3,15] In contrast, perylenediimide (PDI) derivatives are an attractive alternative to fullerenes because they have low-lying LUMO levels, are chemically and environmentally robust (some have been used as automotive paint pigments), and have high electron mobilities.[16−18] Equally important, they have major advantages when compared to fullerenes in having large optical transition dipoles in the solar spectral region, and are synthetically straightforward to modify, offering a wide range of electronic and solid-state packing properties.[16,18,19] Furthermore, they are inexpensive to synthesize and purify on a large scale.[20]
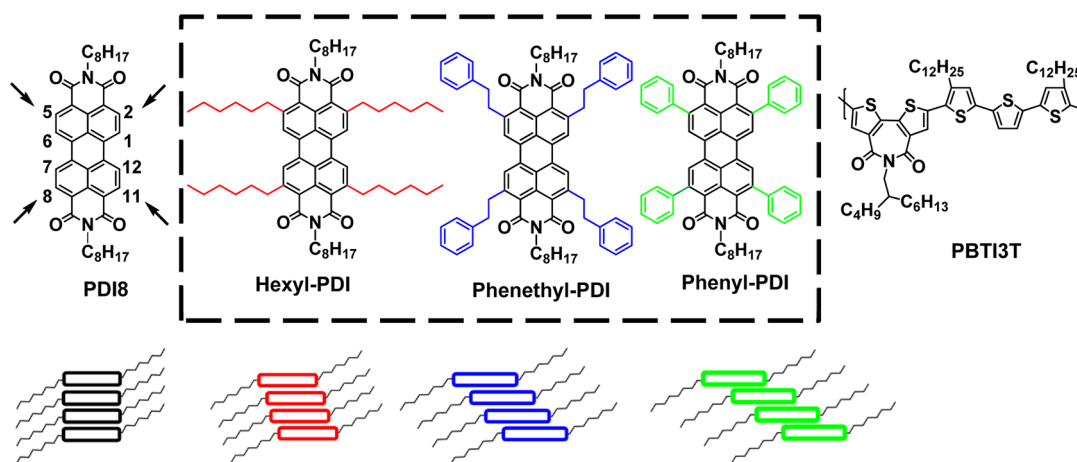
Figure 1. Structures of the PDI acceptors and the donor polymer used in this Article. The headland positions of PDI (C2, C5, C8, and C11) are denoted by arrows in the **PDI8** structure. The possible molecular packing structure of each of the PDIs is also shown. The relative slip angles of **Hexyl-PDI** and **Phenethyl-PDI** are unknown but are hypothesized to follow the trend shown in the figure.

Although PDIs have been investigated in OPVs for more than a decade, including in the very first bilayer devices, and despite their very favorable chemical and electronic properties, PDIs have historically performed poorly in BHJ solar cells.[21,22] One major obstacle has been that many PDI derivatives do not form good bulk-heterojunction morphologies. Because of their extended π-surfaces, PDIs are strongly aggregated in the solid state, and when cast into films form large crystallites that can be micrometer in length.[23] Such behavior translates into BHJ domains that are too large for efficient exciton splitting. While exciton lifetimes and diffusion lengths are quite large in some PDIs, many PDI derivatives tend to form excimers that act as traps for excitation energy. Furthermore, because typical exciton diffusion lengths in donor materials are on the order of 10 nm, large fractions of the excitons are quenched in films having large domain sizes, before reaching a donor−acceptor interface for carrier creation.[1,24−27]

Recent efforts to minimize the formation of such unfavorably large PDI BHJ domains and rapid excimer formation have focused on three major strategies, all yielding substantially improved OPV performance: (1) creating twisted PDI dimers attached at the imide position via a hydrazine linker, (2) creating twisted PDI dimers attached at the 1,6,7,12-positions ("bay positions", see **PDI8** in Figure 1) either directly or with a spacer, and (3) using bulky "swallow tail" PDI side chains at the imide position to introduce twisting in the packing structure.[28−32] Specifically, Narayan et al. reported that a PDI dimer linked through the imide position inhibits excimer formation, leading to OPV PCEs that are 20× those observed in the corresponding PDI monomer, and affording a PCE of 3.2%.[28,33] Similarly, it has been shown that the direct attachment of two PDIs through the bay position results in a dimer in which the individual chromophore π-planes are twisted ∼70° relative to one another.[30] This twist inhibits strong π-stacking and excimer formation, and yields OPV PCEs near 6%.[34] High performance can also be achieved by adding a thiophene linker at the bay position, resulting in a 4.03% efficiency, which can be increased to 4.34% by tuning the active layer donor−acceptor distribution.[31,32] Interestingly, it has also been demonstrated that by mixing the simple *N,N*-bis(3-aminopentyl)PDI, which can be synthesized in good yields in a single step, with different donor materials, PCEs up to 3% can be achieved.[29,35]

Although the strategy of using twisted PDI dimers has resulted in the highest published PCEs for any nonfullerene OPVs to date, it is not without limitations. In the solid state, PDI charge transport is highly anisotropic with high mobilities along the π-stacking direction and far lower mobilities in the transverse direction, whereas the high performance of fullerenes has been attributed to their tendency to isotropically transport charge in all directions.[11,20] Solar cell performance can be maximized only when charge separation and charge collection are both efficient. Photogenerated free charge carriers can be trapped and undergo fast recombination in the absence of a continuous pathway to the collecting electrode with appreciable mobility.[17,36,37] By disrupting close, ordered PDI packing when using twisted dimers, electron mobility is also likely compromised. An alternative approach to the requisite BHJ nanometer scale morphology while still retaining the electronic connectivity required for free charge conduction is to use polymeric acceptors. Several groups have implemented PDI-containing polymers, which results in seemingly good morphology and long-range order. However, OPV performance is not significantly improved in these systems.[24,38−42]

An ideal BHJ acceptor system should preserve the long-range π-stacking characteristics of PDI while simultaneously disrupting excimer formation. Here, we propose a new approach to addressing this challenge by introducing substitutions at the "headland" (C2, C5, C8, and C11) positions of **PDI8** (see Figure 1). Excimer formation has been shown to be rapid in H-aggregated PDI systems, occurring with a time constant as low as 215 fs, but far slower in J-aggregated systems where the exciton diffusion length has been measured to be ∼96 nm.[27,43] In fact, in cofacial dimers, the excimer formation rate in a slip-stacked dimer has been shown to be an order of magnitude slower than that in a completely cofacial dimer.[44] Substitution at the headland positions takes advantage of this because headland substituted PDIs have been shown to organize in slip-stacked structures, resulting in the inhibition of excimer formation, without completely disrupting π-stacking.[45] Another benefit of headland substitutions is that they greatly increase the solubility of PDI without resulting in a core twist, allowing solution processability in systems without branched side chains.[46,47] Slip-stacking behavior can be achieved in several PDIs without core substitution; however, core unsubstituted systems are generally too insoluble for solution processing

unless they have bulky solubilizing groups at the N positions disrupting π-stacking.[48,49] For this reason, slip-stacked PDIs have not been commonly investigated in solution-processed bulk heterojunction solar cells.

EXPERIMENTAL METHODS

Materials Synthesis. All materials were synthesized and characterized according to modified literature procedures. The details of the synthesis and characterization are provided in the Supporting Information.

OPV Device Fabrication. Inverted organic OPV devices with the structure ITO/ZnO/Active Layer/MoO_3/Ag were fabricated according to published literature procedures.[14] The details of device fabrication and optimization are summarized in the Supporting Information.

OTFT Device Fabrication and Testing. Top-gate bottom-contact devices were fabricated in a nitrogen glovebox by spin-coating 5 mg/mL $CHCl_3$ semiconductor solutions filtered through 0.2 μm PTFE filters (2000 rpm) on thermally evaporated gold source/drain electrodes (~50 nm thick, glass substrate). This film was baked at 110 °C for 10 min. Next, the Cytop dielectric layer (CTL-809M) was spin coated at 2000 rpm and the film baked at 110 °C for 10 min. The device structure was completed by thermal deposition of the Au gate electrode. All three PDI-based devices were tested in ambient conditions, and the Phenyl-PDI device was also tested under vacuum. TFTs based on the PBTI3T:Phenyl-PDI semiconductor blend (donor:acceptor ratio of 1:1) were also fabricated, and both electron and hole mobilities were measured in ambient conditions.

Steady-State Spectroscopy. Steady-state optical absorbance spectra were measured using a Shimadzu UV-1800 spectrometer. Fluorescence spectra were measured using a Photon Technology International photon-counting spectrofluorometer. Film samples were spin-coated on glass coverslips following the same procedure as was used for the active layers in device preparation. Film fluorescence measurements were carried out directly on the films, which were placed at a 20° angle to the excitation beam.

Femtosecond Transient Absorption Spectroscopy (fsTA). The details of the transient absorption instrumentation and experimental methodology have been reported previously.[45] Briefly, for visible and near-infrared fsTA, samples were excited at 532 nm with 0.5 μJ/pulse at 1 kHz. The excitation pulse was focused to a 3 mm diameter spot size for film samples to minimize the excitation density and avoid singlet annihilation.

GIWAXS. Grazing incidence X-ray scattering (GIWAXS) measurements were carried out at Beamline 8-ID-E of the Advanced Photon Source at Argonne National Laboratory.[50] Detailed experimental and data analysis procedures are given in the Supporting Information.

RESULTS

In this contribution, we report the synthesis and characterization of three headland substituted PDIs, N,N-bis(n-octyl)-2,5,8,11-tetra(n-hexyl)-PDI (**Hexyl-PDI**), N,N-bis(n-octyl)-2,5,8,11-tetraphenethyl-PDI (**Phenethyl-PDI**), and N,N-bis(n-octyl)-2,5,8,11-tetraphenyl-PDI (**Phenyl-PDI**) (Figure 1), as potential new acceptors for BHJ OPVs. The neat molecules and blend films are characterized by UV–vis optical spectroscopy, cyclic voltammetry, fluorescence spectroscopy, GIWAXS, and AFM. Next, inverted architecture BHJ OPV devices are fabricated using the high-efficiency donor polymer **PBTI3T** (Figure 1). To understand striking OPV performance variations across this PDI series, the resulting BHJ blend morphologies and microstructures are characterized in detail by AFM, TEM, and GIWAXS, while blend charge separation and recombination dynamics are examined using photoluminescence quenching and femtosecond transient absorption spectroscopy. It will be seen that **PBTI3T:Phenyl-PDI** has the deepest lying LUMO, intermediate crystallinity, and the most well-mixed

BHJ domains. This minimizes geminate recombination and affords the highest PCE of 3.67%.

Materials Synthesis and Optoelectronic Properties Characterization. The three PDIs, **Hexyl-PDI**, **Phenethyl-PDI**, and **Phenyl-PDI**, were synthesized via Ru-catalyzed C−H coupling procedures.[46,47] Unlike the unmodified **PDI8**, all three new PDIs are soluble in common organic solvents including dichloromethane, chloroform, dichlorobenzene, and toluene. Optical absorbance spectra of the films cast from chloroform and cyclic voltamograms (CVs) obtained in dichloromethane solutions are shown in Figure 2a,b. Data for the three PDIs are
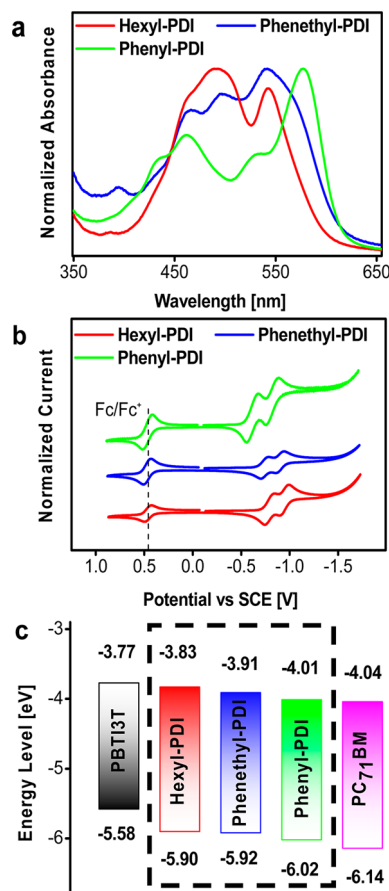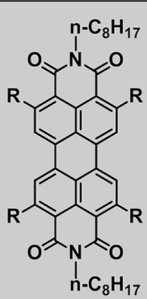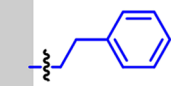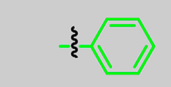

Figure 2. Optoelectronic properties of the present acceptor molecules and donor polymers: (a) Optical absorption spectra of films spun-cast from chloroform with 0.5% diiodooctane by volume. (b) Solution CVs of the PDI acceptors in CH_2Cl_2. (c) Estimated frontier molecular orbitals of the present PDI acceptors along with $PC_{71}BM$ and donor polymers.

summarized in Table 1, along with that of the benchmark n-type material $PC_{71}BM$. The estimated HOMO and LUMO energy levels of the acceptors and the donor polymer **PBTI3T** are also shown in the energy diagram in Figure 2c.

Each of the PDIs undergoes two quasi-reversible reduction events, and none show any oxidative activity in the scan range. The reduction potentials of **Hexyl-PDI**, **Phenethyl-PDI**, and **Phenyl-PDI** are −0.67, −0.77, and −0.85 V vs SCE, respectively, corresponding to LUMO energies of −4.01, −3.91, and −3.83 eV. Note that the LUMO energy of **Phenyl-PDI** is very similar to that of $PC_{71}BM$, −4.04 eV. The optical band gaps (E_g) of **Hexyl-PDI**, **Phenethyl-PDI**, and **Phenyl-PDI** films follow a trend similar to that of the LUMOs,

Table 1. Summary of PDI Optoelectronic Properties

R	Name of Material	LUMO[a] [eV]	HOMO[b] [eV]	λ_{Abs}[c] [nm]	E_g[d] [eV]
	Hexyl-PDI	-3.83	-5.90	492 541 463	2.07
	Phenethyl-PDI	-3.91	-5.92	542 496 465	2.01
	Phenyl-PDI	-4.01	-6.02	577 461 532 435	2.01
	PC$_{71}$BM	-4.04	-6.14		2.09

[a]LUMO energy level of the materials was measured via solution CV. [b]HOMO levels were calculated by subtracting the LUMO level from the optical band gap. [c]The absorbance peaks (λ_{Abs}) of the film. [d]The optical band gap (E_g) calculated from the band edge of the films.
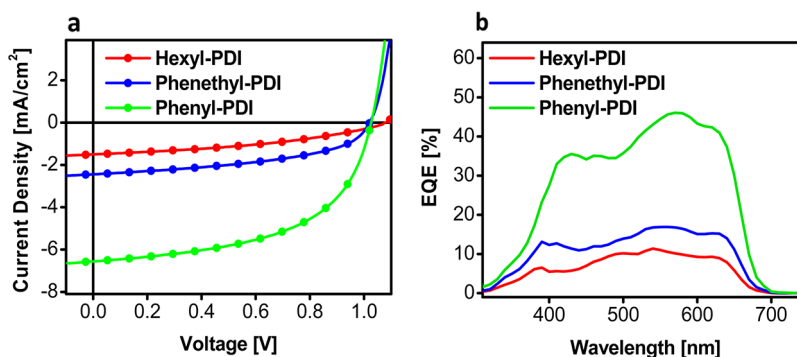

Figure 3. $J-V$ (a) and EQE (b) curves of champion devices of the three PDI acceptors when blended with the donor polymer **PBTI3T**. About 60 nm thick active layers were cast from chloroform with 0.5% DIO.

with **Phenyl-PDI** having the smallest gap (618 nm, 2.01 eV) and **Hexyl-PDI** the largest (600 nm, 2.07 eV). The absorbance maxima (λ_{max}) of the three molecules also follow the same trend. Thus, λ_{max} of **Phenyl-PDI** is the most red-shifted at 577 nm, and that of **Phenethyl-PDI** is next at 542 nm. While **Hexyl-PDI** also has a peak at 541 nm, its λ_{max} is blue-shifted to 492 nm.

Device Fabrication and Evaluation. Inverted solar cells of the structure ITO/ZnO/**PBTI3T:PDI**/MoO$_3$/Ag were fabricated from **PBTI3T:Hexyl-PDI**, **PBTI3T:Phenethyl-PDI**, and **PBTI3T:Phenyl-PDI** BHJ blends (Figure 3). The device performance parameters for the three blends under the optimized fabrication conditions are summarized in Table 2. Devices incorporating the blends of the three different acceptors show marked variations in PCE. The highest PCE of 3.67% is obtained from a **PBTI3T:Phenyl-PDI** "champion cell" where the average PCE is 3.60%. In contrast, the PCE of a

Table 2. Solar Cell Performance of Champion Cells[a]

acceptor	V_{oc} [V]	J_{sc} [mA/cm^2]	FF [%]	PCE[b] [%]
Hexyl-PDI	1.076	1.51	39.29	0.65 (0.58)
Phenethyl-PDI	1.016	2.44	48.48	1.20 (1.15)
Phenyl-PDI	1.024	6.56	54.59	3.67 (3.60)

[a]Active layers were ~60 nm thick with a donor:acceptor ratio of 1:1 and were cast from chloroform solutions that contained 0.5% DIO by volume. [b]Average PCE of four cells is given in parentheses.

champion **PBTI3T:Phenethyl-PDI** device is 1.20% with an average efficiency of 1.15% over four devices, while the PCE of a champion **PBTI3T:Hexyl-PDI** cell is lower at 0.65%, with an average of 0.58%. Interestingly, while the open circuit voltages (V_{oc}) of all three devices types are large and similar (1.016–1.076 V), the short circuit current densities (J_{sc}) and fill factors (FF) of the **Phenethyl-PDI** and **Hexyl-PDI** devices are significantly lower than those of the **Phenyl-PDI** devices. All three blends respond to light within a similar wavelength range, 300–685 nm. However, **PBTI3T:Phenyl-PDI** has the highest conversion efficiency at all wavelengths with EQEs between ~35% and ~45% throughout the 350–750 nm range, with a peak EQE of 46% attained at 570 nm. In contrast, the highest EQE attained by **PBTI3T: Phenethyl-PDI** is 17% at 550 nm, while the highest attained by **PBTI3T:Hexyl-PDI** is only 11% at 540 nm (Figure 3).

TFT devices were fabricated to measure the carrier mobility in pristine films of the PDI materials as well as in the champion **PBTI3T:Phenyl-PDI** blend. The results are summarized in Table 3, and I/V curves are shown in the Supporting Information (Figure S7). Importantly, the electron mobilities for the pristine films follow the performance trend observed for the OPV blends, with the **Phenyl-PDI**-based TFTs exhibiting the highest mobility (2.4×10^{-3} cm^2 V^{-1} s^{-1} in ambient and 2.8×10^{-3} cm^2 V^{-1} s^{-1} in vacuum) followed by the **Phenethyl-PDI** (4.2×10^{-4} cm^2 V^{-1} s^{-1} in ambient) and then by the **Hexyl-PDI** (1.0×10^{-4} cm^2 V^{-1} s^{-1} in ambient) devices. The electron mobility of **Phenyl-PDI** dropped substantially in the blend,

Table 3. OTFT Performance[a]

	μ_e (cm² V⁻¹ s⁻¹) ambient (vacuum)	μ_h (cm² V⁻¹ s⁻¹) ambient
Hexyl-PDI	1.0×10^{-4}	
Phenethyl-PDI	4.2×10^{-4}	
Phenyl-PDI	2.4×10^{-3} (2.8×10^{-3})	
PBTI3T:Phenyl-PDI	4.2×10^{-5}	1.7×10^{-2}

[a]All devices were top-gate bottom-contact and were fabricated and tested as described in the Experimental Methods.

while the hole mobility of **PBTI3T** was comparable to those reported for the same polymer backbone.[14]

Film Morphology and Crystallinity. Possible relationships between thin film properties and the solar cell performance were investigated by studying the morphology and crystallinity of the neat polymer and PDI films and the polymer:PDI BHJ blend films. AFM and 2D GIWAXS images are shown in Figure 4a,b, respectively. Among the PDIs, **Hexyl-PDI** is by far the most crystalline, displaying the largest crystalline domains (1–2 μm), greatest surface roughness (4.2 nm RMS), and the most intense GIWAXS scattering peaks. **Phenyl-PDI** films are of intermediate crystallinity; it does not form micrometer-sized crystallites, but the surface is still rather

rough (3.7 nm RMS) and GIWAXS images still display discrete reflections. **Phenethyl-PDI** and **PBTI3T** form very smooth films and show broad amorphous peaks in the GIWAXS patterns. When the PDIs are blended with the donor polymer, the resulting films become significantly smoother than the corresponding neat PDI films. However, as in the case of the neat films, **Hexyl-PDI** forms the roughest and **Phenethyl-PDI** forms the smoothest films. The blend films also lack the sharp GIWAXS reflections present in the neat PDI films, indicating loosening of local PDI crystalline packing.

The GIWAXS data can be further analyzed by resolving into constituent horizontal (in-plane or xy) and vertical (out-of-plane or z) linecuts, as shown in Figure 5a,b. In both horizontal and vertical directions, for each of the films, two sets of reflections are evident. The first set at 0.2 Å⁻¹ < q < 0.6 Å⁻¹ (or 10–31 Å), identified in the figure by arrows, corresponds to the polymer and the PDI lamellar stacking planes that are formed due to side-chain interactions. The second set around q = 1.7 Å⁻¹ (or 3.7 Å), as highlighted by the square brackets, corresponds to the reflection planes that are formed by the π-stacking interactions of the polymer and the PDIs. The π-stacking peaks that appear in the out-of-plane direction correspond to the face-on orientation of the stacks on the substrates.[51] When molecules and polymers orient face-on on
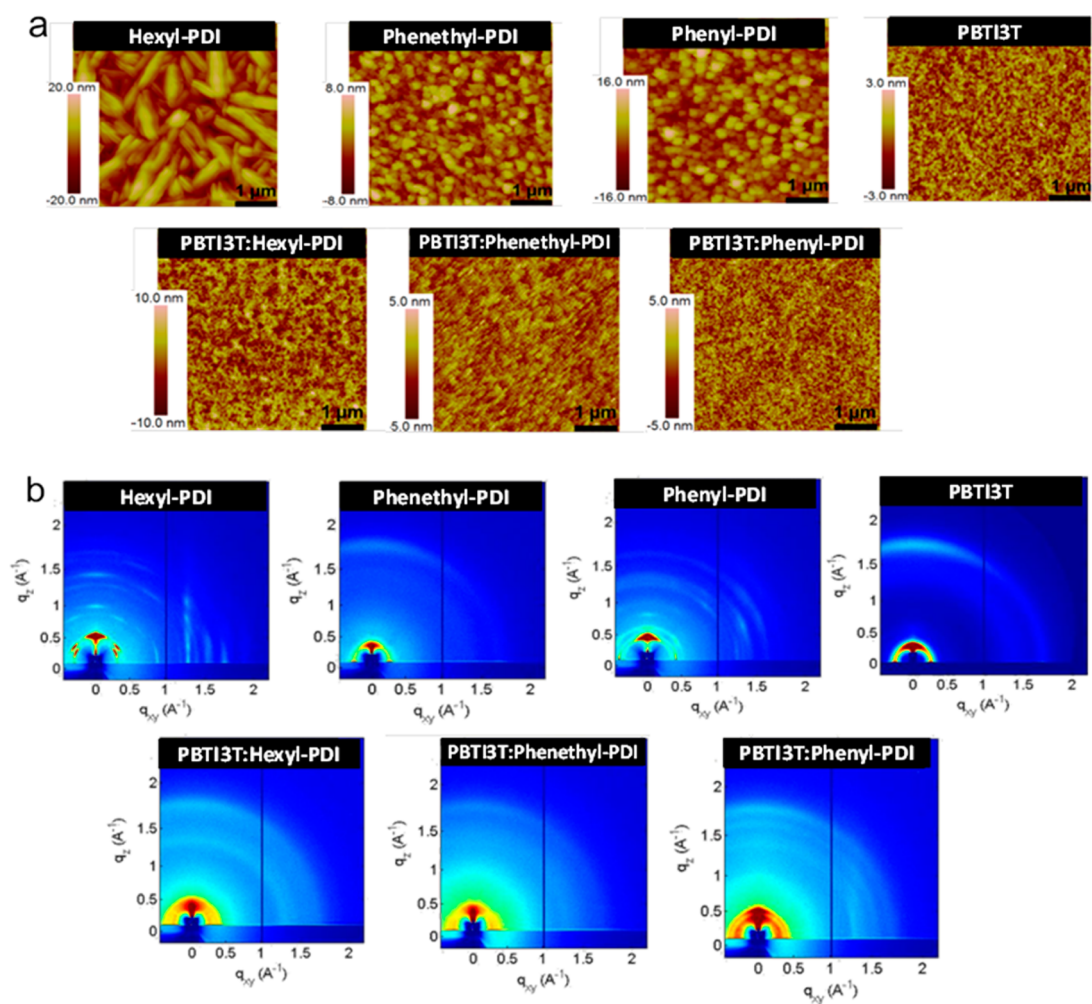

Figure 4. (a) AFM images of neat and blend films. RMS roughnesses for the neat films of **Hexyl-PDI**, **Phenethyl PDI-**, **Phenyl-PDI**, and **PBTI3T** are 4.2, 1.6, 3.7 and 0.6, respectively. The RMS roughnesses of the **PBTI3T:Hexyl-PDI**, **PBTI3T:Phenethyl-PDI**, and **PBTI3T: Phenyl-PDI** blends are 2.3, 0.8, and 1.0 nm, respectively. (b) 2D GIWAXS images of the neat and the blend films.
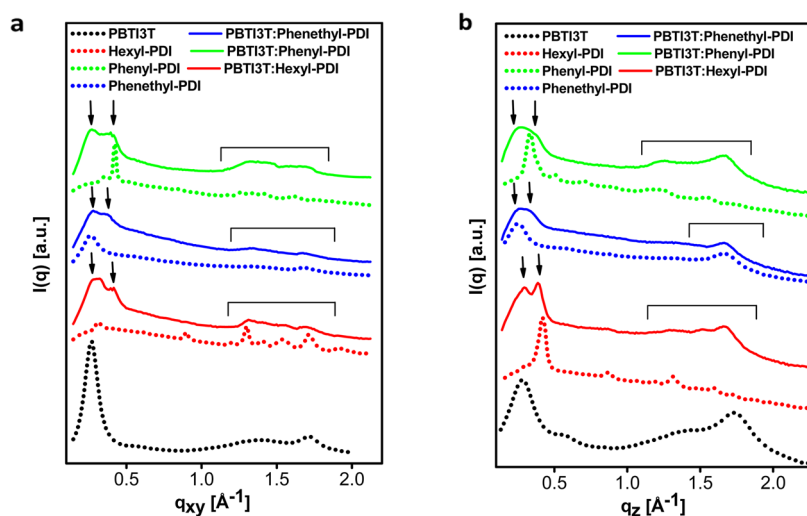
Figure 5. In-plane (a) and out-of-plane (b) GIWAXS linecuts of the neat **PBTI3T**, **Hexyl-BTI**, **Phenethyl-PDI**, and **Phenyl-BTI** films and of the donor:acceptor blends.
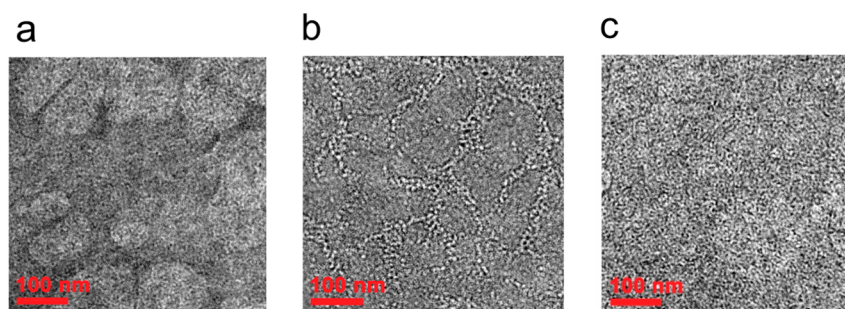

Figure 6. TEM images of (a) **PBTI3T:Hexyl-PDI**, (b) **PBTI3T:Phenethyl-PDI**, and (c) **PBTI3T:Phenyl-PDI** BHJ blend films.

the substrate surface, their side chains typically interdigitate and lie parallel to the surface. This results in a corresponding side-chain interaction peak in the horizontal direction.[48] **PBTI3T** exhibits a face-on π-stacking peak at $q_z = 1.73$ Å^{-1} and a corresponding lamellar peak at $q_{xy} = 0.27$ Å^{-1}. This corresponds to a π-stacking distance of 3.63 Å and a backbone stacking distance of 23.3 Å, metrics that are in very close agreement with reported values for similar systems.[14] Among the neat PDI films, **Phenethyl-PDI** displays a clear π-stacking peak ($q_z = 1.66$ Å^{-1}, $d = 3.78$ Å), whereas the **Hexyl-PDI** and **Phenyl-PDI** films exhibit several crystalline reflections in the π-stacking region. When blended with the PDIs, the polymer π-stacking peak is evident at $q_z = 1.67$ Å^{-1} ($d = 3.76$ Å), with the stacking distance slightly larger than that in neat **PBTI3T** films.

In contrast to what is observed for face-on stacking, the present peaks at $q_{xy} \approx 1.7$ Å^{-1} and 0.2 Å^{-1} < q_z < 0.6 Å^{-1} represent molecules oriented edge-on to the substrate surface. Comparing the face-on and edge-on metrics gives a semi-quantitative measure of the relative orientation of the crystallites in the film. The stacking distances and correlation lengths from Scherrer analysis of the lamellar stacking peaks of the PDI and **PBTI3T** neat and blend films are summarized in Supporting Information Table S2.[52] The neat **PBTI3T** films exhibit a preferential face-on orientation with a face-on to edge-on (f:e) ratio of 2.2:1.0, in agreement with the literature.[14] The neat **Phenethyl-PDI** films show predominantly amorphous features but also exhibit a clear π-stacking peak with an f:e ratio of 2.1:1.0. Furthermore, the neat **Phenyl-PDI** and **Hexyl-PDI** films show relatively strong crystallinity as compared to the

Phenethyl-PDI and the **PBTI3T** neat films, and the correlation lengths of the **Phenyl-PDI** and **Hexyl-PDI** films are greater than 10 nm, as compared to correlation lengths of ~5 nm for **Phenethyl-PDI** and **PBTI3T**. However, preferential orientation is difficult to quantify due to large number of reflections in the π-stacking region. Although orientation was not determined, the neat films of **Phenyl-PDI** and **Hexyl-PDI** do show a strong preferential orientation as demonstrated by well-defined reflections, whereas the scattering patterns for **Phenethyl-PDI** and **PBTI3T** are far more isotropic. Furthermore, the scattering data for **Phenyl-PDI** match a simulated powder pattern based on the reported crystal structure (Supporting Information Figure S4).[45] This means that the **Phenyl-PDI** molecules retain their slip-stack packing behavior within the larger crystalline domains of the corresponding films.

Note also that the **PBTI3T** components of all of the present BHJ blend films exhibit enhanced face-on orientation, similar to the behavior previously observed for **PBTI3T**:fullerene blends.[14] In fact, the **PBTI3T** edge-on π-stacking reflection cannot be observed in any of the blend film data. Scherrer analysis of the lamellar peaks in the blend films reveals that the correlation lengths of the PDIs decrease upon the addition of the polymer in all three cases, whereas the **PBTI3T** correlation length is approximately unchanged in the **PBTI3T:Phenyl-PDI** and the **PBTI3T:Hexyl-PDI** blends but is increased in the case of **PBTI3T:Phenethyl-PDI**.

The nanoscale morphology of the donor:acceptor blends was also investigated by TEM (Figure 6). The **PBTI3T:Phenyl-PDI** films appear to be very homogeneous with small crystalline
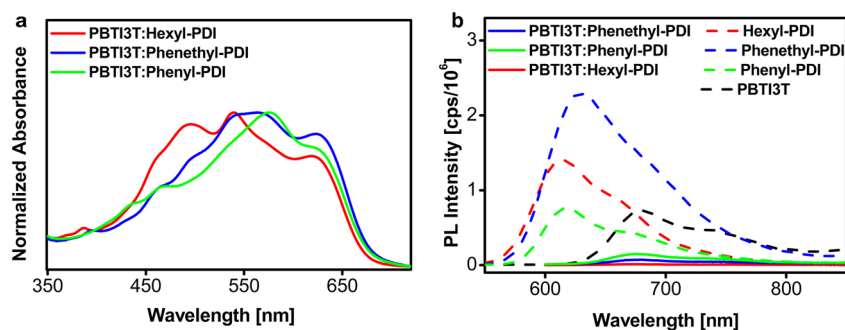
Figure 7. (a) Normalized optical absorbance spectra of the donor:acceptor blend films and (b) photoluminescence (PL) spectra of the neat and blend films.
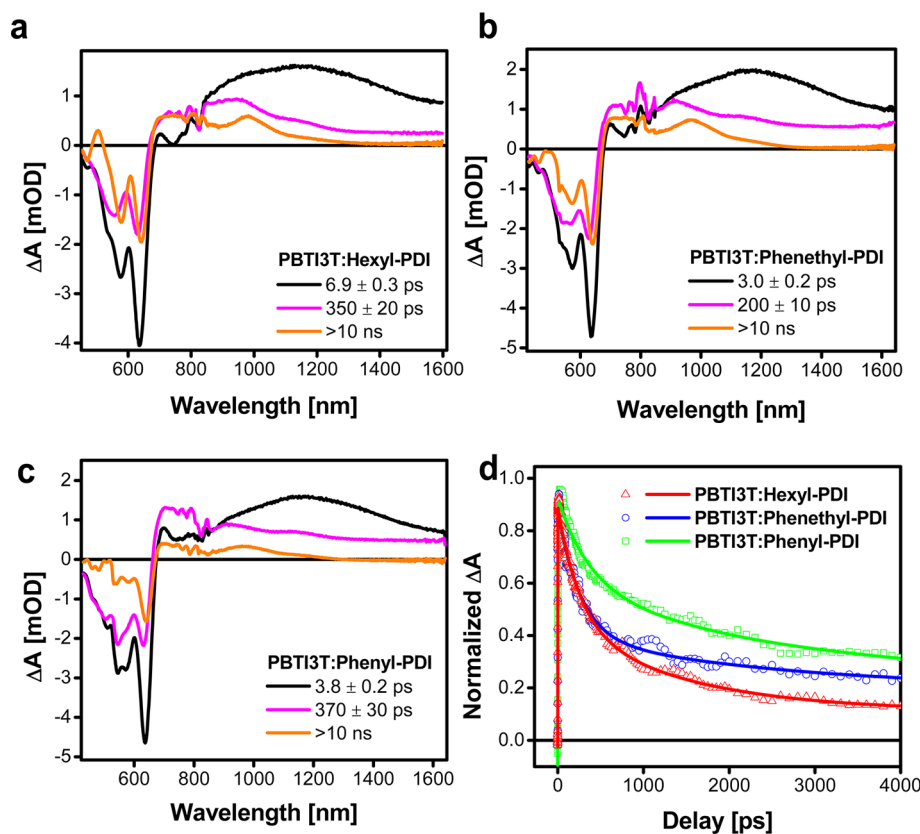

Figure 8. Global fits of fsTA data for **PBTI3T:Hexyl-PDI**, **PBTI3T:Phenethyl-PDI**, and **PBTI3T:Phenyl-PDI** blend films at different time intervals (a−c); and the kinetic fits of the PDI anion absorbance in the three blends between 700 and 900 nm (d).

grains (∼2−5 nm in size), uniformly covering the entire scan area. In contrast, the **PBTI3T:Hexyl-PDI** films appear less homogeneous and show features extending ∼100 nm. In contrast, the **PBTI3T:Phenethyl-PDI** films are devoid of any large features but exhibit large amorphous regions scattered over the scan area.

Charge Separation and Charge Recombination Dynamics. Photoluminescence (PL) experiments (Figure 7) reveal that each of the present three PDIs almost entirely quenches the fluorescence of **PBTI3T** BHJ films. Quenching efficiencies of 99%, 97%, and 89% are measured for the **PBTI3T:Hexyl-PDI**, **PBTI3T:Phenethyl-PDI**, and **PBTI3T:-Phenyl-PDI** blend films, respectively. Such low PL quantum yields suggest that excitons in each of the blends travel to the donor:acceptor interface and are separated with high efficiency.

The charge separation and recombination behavior of the three blends were further investigated with femtosecond

transient absorption spectroscopy (fsTA). Transient spectra and recombination rates for **Hexyl-PDI**, **Phenethyl-PDI**, **Phenyl-PDI**, and **PBTI3T** neat films, as well as the transient spectra for the blend films, are provided in the Supporting Information (Figures S5,S6). Global fitting of the fsTA data via singular value decomposition (SVD) methods reveals the existence of three species in each of three blends. The species associated spectra are shown in Figure 8a−c. The first species decays with a time constant of 3−7 ps and is assigned to **PBTI3T** excitation. The second species decays with a time constant of 200−370 ps and is assigned to a population of trapped geminate radical pairs, which undergo rapid charge recombination. The third and the final species lives for the length of the experiment and is assigned to fully separated charge carriers. Kinetic fits of the PDI anion region for the blend films are also shown in Figure 8d and support the time constants extracted from the global fitting.
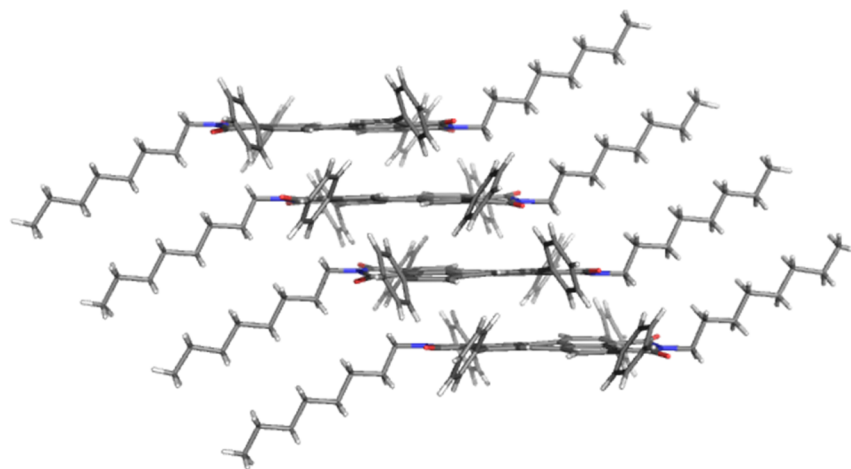
Figure 9. Diffraction-derived crystal structure of **Phenyl-PDI** showing the close slip-stacked packing.[44] The slip angle along the long axis of the PDI core is 47°. The crystal structures of **Phenethyl-PDI** and **Hexyl-PDI** could not be determined because diffraction-quality crystals could not be grown.

DISCUSSION

PDIs can be synthetically modified at the imide N-positions, the "bay" positions, or the "headland" positions. The most commonly studied PDI derivatives are substituted at the imide and the bay positions. This is because substitution at the headland positions was difficult until the development of efficient Ru-catalyzed C−H activation methodologies.[46,47] Unlike substitution in the imide N positions, which has a minimal effect on PDI electronic properties, and substitution in the bay positions, where controlling electron-donating properties can be complicated by a substituent-induced core-twisting, PDI substitution at the headland positions can result in large electronic properties changes while maintaining core planarity.[18]

Phenyl-PDI crystallizes in a slip-stacked motif, which is preserved in vapor-deposited[45] and, as this work shows, solution-deposited thin films (Figure 9, Supporting Information Figure S4). Photoexcitation of these films results predominantly in singlet exciton fission with small amounts of competing excimer formation. Singlet exciton fission is undesirable in OPVs that are not specifically designed to take advantage of it because the resultant triplet excitons are quite low in energy and therefore unable to undergo efficient charge separation. However, the rate of singlet exciton fission in these films is slow and the rate of excimer formation is even slower, resulting in singlet exciton lifetimes on the order of 200 ps, which is significantly longer than in systems with rapid excimer formation such as in most PDI films.[27,53] Furthermore, the rate of charge separation in BHJs is generally much faster than 200 ps, meaning that headland substituted PDIs may provide a potential solution to the undesirable excimer formation observed in other PDIs. Headland substituted PDIs have been used in solar cells before; however, in that case, an N-swallowtail substituent was used to disrupt slip-stacking behavior, thus resulting in a packing motif with very little π-overlap.[46,47] This structural limitation is consistent with the modest PCE of 0.50% observed in BHJ OPVs fabricated with that material.[54] Additionally, that system used alkyl substituents in the headland positions that, as shown here, raise the LUMO energy, which may disfavor charge separation.

The steady-state optical absorption spectra of the present PDI thin films also reveal interesting information about packing

in the solid state. The intermolecular packing motifs proposed in Figure 1 for two of the molecules, the columnar structure of **PDI8** and slip-stacked structures of **Phenyl-PDI**, are derived from their known crystal structures. The crystal structures of **Phenethyl-PDI** and **Hexyl-PDI** could not be obtained as they did not form diffraction quality crystals but instead formed long very fine fibers (∼1 μm in diameter and several hundred micrometers in length), suggesting a strong interaction in one direction. This is likely a result of the strong π-stacking interactions commonly observed in PDI derivatives.[55] On the basis of the structures and the absorption spectra of these molecules, we hypothesize that the relative slip angles in the PDIs are as shown in Figure 1, with the **Phenyl-PDI** being the most slipped, the **Phenethyl-PDI** having an intermediate slip angle, and finally the **Hexyl-PDI** being the least slipped. The effect of crystal packing on the optical absorption of PDI has been well studied, and calculations by Engels et al. suggest that a longitudinal displacement of 3.5 Å (as observed in the crystal structure of **Phenyl-PDI**) should result in an increasing band gap with decreasing slip angle.[56] This trend in the slip angle can be explained in terms of the steric bulk of the different headland substituents. Thus, the encumbrance of the phenyl ring is greater than that of the phenethyl group, which in turn is greater than that of an *n*-hexyl group. It is important to note that despite the change in molecular packing, hypothesized here to decrease the slip angles, both **Phenethyl-PDI** and **Hexyl-PDI** exhibit some vibronic structure in steady-state fluorescence (Figure 7). These vibronic structures are characteristic of monomer-like fluorescence and are not observed in systems with rapid excimer formation, where broad fluorescence spectra with larger Stokes shifts are observed.[57] Additionally, despite the decreased slip angle in **Phenethyl-PDI** and **Hexyl-PDI**, the excited-state lifetimes of all three films are greater than 100 ps, which should be sufficient for long distance exciton diffusion. These results suggest that all three molecules successfully inhibit excimer formation in the solid state. We propose that this is the result of a slip-stacked packing geometry. This mechanism is consistent with that observed in solution for dimers and solution aggregates.[27,44] Slip-stacking has also been observed in crystals of "bare" PDIs without substituents on the headland or bay positions, but as far as we know the effect of

packing geometry in these systems on the rate of excimer formation has not been systematically investigated.

The solar cell performance of many different donor−acceptor blends, including those with PDI-based acceptors, has been optimized using processing additives such as 1,8-diiodooctane (DIO).[9,14,29,31,58,59] In the present study, small amounts of DIO (0.5% by volume) significantly enhance the performance of the **PBTI3T:Phenyl-PDI** blend OPVs, probably because of increased microstructural order in the blend. However, increasing the DIO concentration further results in the formation of very large (>100 nm, Supporting Information Figure S3) PDI crystallites and consequently lowered OPV performance. Solar cell performance data for different active layer DIO concentrations as well as the AFM, TEM, and GIWAXS images of the films are summarized in the Supporting Information. Device performance was also optimized for active layer thickness. The highest performance was obtained for 60 nm thick films. Thinner films result in higher fill factors (more efficient current collection) but decreased absorbance and hence yielded lower short-circuit currents. Thicker films afford lower fill factors and lower currents, presumably because of increased resistance.

Besides a favorable morphology, another important consideration in the design of a PDI-based OPV acceptor is the electron affinity, or LUMO energy. Charge separation in organic solar cells is driven by the energy offset between the donor and acceptor LUMO levels.[60,61] Literature reported high-performance PDI-based solar cells often have moderate to large LUMO−LUMO offsets between the donor and acceptors (0.6−0.8 eV).[31,33] While such a strategy might assist charge separation, it is not without drawbacks because it results in energy loss in the form of V_{oc} depression. Obtaining efficient charge separation without significant V_{oc} losses is ideal. Recent literature reports show that a low driving force is sufficient for efficient charge separation in fullerene-based system by exploiting "hot excitons" and/or by delocalization of charge carriers.[61,62] The present study shows that headland-substituted PDIs are capable of undergoing rapid charge separation in a BHJ blend and that they have easily tailorable energetics and slip-stacked packing structures. The LUMO level can be predictably tuned by exploiting the electron-donating strength of the various substituents because of the strong electronic coupling between the PDI core and headland substituents. Interestingly, the LUMO energy of **Phenyl-PDI** determined electrochemically is very similar to that of $PC_{71}BM$ (−4.01 and −4.04 eV, respectively). This suggests that, as far as energy level requirements are concerned, **Phenyl-PDI** should function well as an alternative acceptor to fullerenes because the difference in the energy between the LUMO orbitals of the donor and that of the acceptor is a measure of the driving force for charge separation.[62] The LUMO energy of **PBTI3T** is −3.77 eV, so ΔG_{CS} can be roughly approximated as −0.24, −0.14, and −0.06 eV for **Phenyl-PDI**, **Phenethyl-PDI**, and **Hexyl-PDI**, respectively.[14] Although this should be sufficient driving force in the case of **PBTI3T:Phenyl-PDI**, it is low for **PBTI3T:Phenethyl-PDI** and **PBTI3T:Hexyl-PDI**.

In terms of OPV performance dependence on acceptor, we observe significant enhancement on going from **Hexyl-PDI** → **Phenethyl-PDI** → **Phenyl-PDI**. This trend is solely due to increases in J_{sc} and FF because V_{oc} for all three blends is very similar (∼1.02−1.076 V). It is of particular note that the V_{oc}'s afforded by the three PDIs reported in this work are significantly higher (by over 0.22 V) than that obtained with

a similar donor polymer, containing an identical core but slightly solubilizing side chains, blended with $PC_{71}BM$.[14] The **PBTI3T:Hexyl-PDI** blends afford low J_{sc} and low FF (1.51 mA/cm^2 and 39.29%) and consequently a low PCE of 0.65%. The **PBTI3T:Phenethyl-PDI** blends afford a slightly higher PCE of 1.20% because of slightly higher J_{sc} (2.44 mA/cm^2) and FF (48.48%) metrics. The PCE afforded by **PBTI3T:Phenyl-PDI** is even higher, up to 3.67%, because of its larger J_{sc} (6.56 mA/cm^2) and FF (54.59%). Interestingly, all three PDI derivatives exhibit high and very similar V_{oc}'s despite having different LUMO levels. This is likely a result of increased nonradiative recombination and resistance in the **PBTI3T:Phenethyl-PDI** and the **PBTI3T:Hexyl-PDI** blends.[63,64] This is supported by the fact that the slope of the J−V curve near open-circuit conditions is steep in the case of the **PBTI3T:Phenyl-PDI** blend and is less steep in the case of the **PBTI3T:Phenethyl-PDI** blend and even less so in the **PBTI3T:Hexyl-PDI** blend.

As shown in the Results, the TFT electron mobility of our PDIs ($\mu_{Phenyl-PDI} > \mu_{Phenetyl-PDI} > \mu_{Hexyl-PDI}$) follows the same OPV performance trends and is comparable to or exceeding those of other nonfullerene acceptors reported in the literature.[65] This trend in mobility could explain the observed trend in fill factor observed as fill factor has been shown to be closely related to the mobility of the active layer materials and to bimolecular recombination.[63,66,67] Additionally, although the pristine electron mobility is comparable to the hole mobility in pristine **PBTI3T**, we observe a significant decrease in electron mobility in the blend film. This likely results in a charge transport imbalance, which limits efficiency improvement and provides a target for further optimization.

While the PL quenching experiments suggest that the three PDIs reported here can efficiently separate charge, this does not explain the differences in OPV performance between the three blends. In fact, the OPV performance trend that would be expected from the PL quenching results is opposite of what is observed experimentally. The trend must therefore reflect the following: (1) differing blend morphologies, (2) differing blend charge recombination features, or (3) some combination of the differing blend morphology and charge recombination characteristics. Here, we discuss these issues in detail.

The morphology/microstructure of the present blends was studied further by AFM, GIWAXS, and TEM. The AFM images reveal that all three films are quite smooth with RMS roughnesses between 0.8−2.3 nm, with **PBTI3T:Hexyl-PDI** being the roughest and the **PBTI3T:Phenethyl-PDI** being the smoothest. It is of particular note that these films are significantly smoother than the corresponding neat PDI films. This result argues that the polymer has weakened the otherwise long-range order in the **Hexyl-PDI** and **Phenyl-PDI** interbackbone packing, in agreement with the GIWAXS-derived PDI correlation lengths, which decrease in both the q_z and the q_{xy} directions of the blends. Not only does the **PBTI3T** break up the large PDI crystallites and consequently generate very smooth films, it does so while still retaining significant face-on π stacking. This combination provides two very advantageous factors for solar cell performance.[14,68,69] Detailed analysis of the morphology of the blends at the nanometer scale via TEM (Figure 5) provides a better understanding of the observed device performances. The TEM image of the **PBTI3T:Hexyl-PDI** blend film shows features ∼100 nm in length, signifying poor mixing and BHJ morphology. Additionally, it appears that the **PBTI3T:Phenethyl-PDI** blend segregates into a nonuni-

form morphology on the nanometer scale, and contains numerous diffuse dark domains that are ∼100 nm across. These large domains have low contrast in the TEM, suggesting that they are likely mixed domains. Considering that we observe quantitative charge separation in the films, it seems likely that these domains are too finely mixed, resulting in charge trapping. In contrast to these results, the **PBTI3T:-Phenyl-PDI** TEM image reveals a homogeneous and well-mixed blend with a uniform distribution of light and dark domains. These domains are only a few nanometers in size and are probably individual **Phenyl-PDI**-rich and **PBTI3T**-rich domains. The presence of these more pure domains could offer an explanation as to why there is less geminate recombination in the **PBTI3T:Phenyl-PDI** blends. It is possible that fine-tuning of the film processing conditions may improve the morphology of both the **PBTI3T:Hexyl-PDI** and the **PBTI3T:Phenethyl-PDI** blends; however, we decided to maintain the processing conditions constant to limit the number of variables considering the wide variety of processing conditions available.

Transient absorption spectroscopy is a powerful technique to interrogate charge generation and recombination phenomena in BHJ films.[70,71] To begin, the spectra of neat **PBTI3T** films show ground-state bleaching, stimulated emission, and a very strong, broad, excited-state absorbance in the NIR centered at 1250 nm. Furthermore, this **PBTI3T** excited-state absorption decays with a time constant of ∼45 ps. The PDI neat films are characterized by much weaker excited-state absorptions centered at 700 nm, which decay in several hundred picoseconds (Supporting Information Figure S5). In marked contrast, the blend films show clear evidence of rapid charge separation. Thus, at very early times, the transient spectra of the blends resemble the **PBTI3T** excited state, characterized by strong NIR absorption. This excited-state absorption rapidly decays with time constants of 3.8, 3.0, and 6.9 ps for the **PBTI3T:Hexyl-PDI**, **PBTI3T:Phenethyl-PDI**, and **PBTI3T:-Phenyl-PDI** blends, respectively. This decay is accompanied by a rise at 750 nm, which is likely due to combined loss of stimulated emission from the **PBTI3T** and the formation of a broad PDI anion absorption feature, consistent with the radical anion absorbance of PDI solution-phase aggregates and covalent dimers (Supporting Information Figure S6).[72,73] There is also an absorption in the NIR centered at 950 nm, which is characteristic of the PDI anion and remains after the decay of the **PBTI3T** excited-state absorption.[74] For these reasons, the time constants are assigned to charge separation in the blend films. Given that **PBTI3T** has an excited-state lifetime of 45 ps, these time constants result in charge separation yields of 92%, 94%, and 87% for **PBTI3T:Hexyl-PDI**, **PBTI3T:Phenethyl-PDI**, and **PBTI3T:Phenyl-PDI** films, respectively. This result confirms that charge separation is responsible for the large extent of PL quenching in the blend films.

The charge recombination rates of the three BHJ blend films are important for understanding why the OPV performance of these materials differs so greatly. All three blends exhibit multiexponential charge recombination. Global fitting of the fsTA data via singular value decomposition (SVD) reveals the existence of three species in each of the blends. Furthermore, the SVD shows that there are two major recombination rates, one fast and one slow. The fast recombination time constants from the SVD analysis are 345, 285, and 370 ps for the **PBTI3T:Hexyl-PDI**, **PBTI3T:Phenethyl-PDI**, and **PBTI3T:-**

Phenyl-PDI blends, respectively (Figure 8a−c). Kinetic fits of the PDI anion peak from 700 to 800 nm give lifetimes similar to those from the SVD analysis (Figure 8d). The blends also have some charge separated population that persists for the length of the experiment. The major difference between the three blends is the yield of long-lived charge separation. These yields track well with the overall PV performance of the BHJ materials and are 19%, 27%, and 36% for **PBTI3T:Hexyl-PDI**, **PBTI3T:Phenethyl-PDI**, and **PBTI3T:Phenyl-PDI**, respectively. The short-lived population most likely decays as a result of geminate pair recombination, while the long-lived population is most likely nongeminate.[36] This suggests that, although a large percentage of excitons undergo charge transfer in all of the films, many are trapped in low-lying geminate states rather than fully dissociating into free charge carriers, which are collected at the cell electrodes.

There are two possible explanations for why the different PDI acceptors in this study afford different free carrier yields. The first concerns the differing morphologies at the donor−acceptor blends. The second concerns the increased driving force for dissociation of bound charge transfer states (CT) into fully separated states (CS). Although all three materials resulted in smooth films with moderate crystallinity, the TEM shows there are striking differences in the nanostructures of the blends. Specifically, while the **PBTI3T:Phenyl-PDI** blend is composed of small domains with high contrast in the TEM, the **PBTI3T:Hexyl-PDI** and **PBTI3T:Phenethyl-PDI** blends are composed of much larger domains with lower contrast (Figure 6). This could be a result of mixing of the PDI into the polymer domains of these blends and vice versa, which could result in the inability of CT states to delocalize and fully separate into free carriers.

Interface morphology has been proposed to underlie subnanosecond charge recombination in all-polymer solar cells, and it has been demonstrated that the donor−acceptor spacing at the interface can have significant effects on charge separation efficiency.[36,75] It has also been demonstrated, for cases when PDI is blended with certain donor polymers, that the barrier for charge separation is greater for PDI as an acceptor than for PCBM.[76] It is possible that this barrier is diminished in PDI systems having bulkier substituents, which maintain greater donor−acceptor separations at the BHJ interface.

It is also possible that excess energy in the initial CT state is used to overcome the charge separation barrier.[77] In this case, it would be logical that the system with the maximum free energy difference would give the highest yield of separation. Specifically, the estimated driving forces for charge separation are −0.24, −0.14, and −0.06 eV for **Phenyl-PDI**, **Phenethyl-PDI**, and **Hexyl-PDI**, respectively. This means that the CT state **PBTI3T:Phenyl-PDI** blend has the most excess energy and therefore the most favorable probability to fully separate. This result could also be explained by increased band-broadening for the **Phenyl-PDI** as compared to the other acceptors. Kazmaier and Hoffman predicted that band broadening qualitatively correlates to the energy and the band broadness of an absorption in the solid state.[49] Because the **Phenyl-PDI** absorption is the most red-shifted and broadest of the three systems, this result suggests the possibility of increased band broadening, which would lead to increased stabilization of charge carriers.

Charge separation in organic solar cells is driven by an energy offset between the donor and the acceptor LUMO

16354

dx.doi.org/10.1021/ja508814z | J. Am. Chem. Soc. 2014, 136, 16345−16356

levels.[60,61] High-performance PDI-based solar cells reported in the literature tend to have large LUMO−LUMO offsets of 0.6−0.8 eV.[31,33] While such a strategy may favor charge separation, it has the disadvantage that it results in energy loss in the form of V_{oc} lowering. Obtaining a high degree of charge separation without significant V_{oc} losses is ideal. Here, we are able to minimize the LUMO−LUMO offset while achieving high V_{oc}'s of ~1.0 V

CONCLUSIONS

Three headland-substituted PDI-based electron acceptors have been synthesized. Detailed characterization reveals that these substituted PDIs have slip-stacked packing, which suppresses excimer formation while preserving good π-stacking for charge transport. The relative proportion of geminate recombination decreases with increasing steric bulk in the headland position and with increasing driving force for charge separation. BHJ devices employing these three acceptors afford high V_{oc}'s (>1.0 V) and relatively high fill factors. The best performing BHJ blend, **PBTI3T:Phenyl-PDI**, affords a PCE of 3.67%. Detailed characterization of the blends using AFM, TEM, and GIWAXS suggests that moderate crystalline size with well-defined nanoscale donor−acceptor domains favors higher PCEs. Transient absorption spectroscopy reveals that the **PBTI3T:-Phenyl-PDI** blend supports higher yields of long-lived charge separated species versus the other two PDI blends, which further contributes to the higher PCE. We believe that these results demonstrate that using slip-stacked PDI acceptors is a useful strategy for designing high-performance nonfullerene OPV acceptors.

ASSOCIATED CONTENT

ⓢ Supporting Information

Experimental details including synthetic methods, electrochemical characterization, GIWAXS characterization, and transient characterization of the neat films. This material is available free of charge via the Internet at http://pubs.acs.org.

AUTHOR INFORMATION

Corresponding Authors
r-chang@northwestern.edu
m-hersam@northwestern.edu
m-wasielewski@northwestern.edu
t-marks@northwestern.edu

Author Contributions
‖P.E.H., A.T., and H.S.S.R.M. contributed equally.

Notes
The authors declare no competing financial interest.

ACKNOWLEDGMENTS

REFERENCES

(1) Günes, S.; Neugebauer, H.; Sariciftci, N. S. *Chem. Rev.* **2007**, *107*, 1324.
(2) Service, R. F. *Science* **2011**, *332*, 293.
(3) Po, R.; Bernardi, A.; Calabrese, A.; Carbonera, C.; Corso, G.; Pellegrino, A. *Energy Environ. Sci.* **2014**, *7*, 925.
(4) Forrest, S. R. *Nature* **2004**, *428*, 911.
(5) Green, M. A.; Emery, K.; Hishikawa, Y.; Warta, W.; Dunlop, E. D. *Prog. Photovoltaics* **2014**, *22*, 701.
(6) You, J.; Dou, L.; Yoshimura, K.; Kato, T.; Ohya, K.; Moriarty, T.; Emery, K.; Chen, C.-C.; Gao, J.; Li, G.; Yang, Y. *Nat. Commun.* **2013**, *4*, 1446.
(7) Yu, G.; Gao, J.; Hummelen, J.; Wudl, F.; Heeger, A. *Science* **1995**, *270*, 1789.
(8) Hoppe, H.; Sariciftci, N. S. *J. Mater. Res.* **2004**, *19*, 1924.
(9) Liang, Y.; Xu, Z.; Xia, J.; Tsai, S.-T.; Wu, Y.; Li, G.; Ray, C.; Yu, L. *Adv. Mater.* **2010**, *22*, E135.
(10) Sun, Y.; Welch, G. C.; Leong, W. L.; Takacs, C. J.; Bazan, G. C.; Heeger, A. J. *Nat. Mater.* **2012**, *11*, 44.
(11) Savoie, B. M.; Rao, A.; Bakulin, A. A.; Gelinas, S.; Movaghar, B.; Friend, R. H.; Marks, T. J.; Ratner, M. A. *J. Am. Chem. Soc.* **2014**, *136*, 2876.
(12) Sariciftci, N. S.; Smilowitz, L.; Heeger, A. J.; Wudl, F. *Science* **1992**, *258*, 1474.
(13) Park, S. H.; Roy, A.; Beaupre, S.; Cho, S.; Coates, N.; Moon, J. S.; Moses, D.; Leclerc, M.; Lee, K.; Heeger, A. J. *Nat. Photonics* **2009**, *3*, 297.
(14) Guo, X.; Zhou, N.; Lou, S. J.; Smith, J.; Tice, D. B.; Hennek, J. W.; Ortiz, R. P.; Navarrete, J. T. L.; Li, S.; Strzalka, J.; Chen, L. X.; Chang, R. P. H.; Facchetti, A.; Marks, T. J. *Nat. Photonics* **2013**, *7*, 825.
(15) Anctil, A.; Babbitt, C. W.; Raffaelle, R. P.; Landi, B. J. *Environ. Sci. Technol.* **2011**, *45*, 2353.
(16) Würthner, F. *Chem. Commun.* **2004**, 1564.
(17) Dittmer, J. J.; Marseglia, E. A.; Friend, R. H. *Adv. Mater.* **2000**, *12*, 1270.
(18) Li, C.; Wonneberger, H. *Adv. Mater.* **2012**, *24*, 613.
(19) Kozma, E.; Catellani, M. *Dyes Pigm.* **2013**, *98*, 160.
(20) Zhan, X.; Facchetti, A.; Barlow, S.; Marks, T. J.; Ratner, M. A.; Wasielewski, M. R.; Marder, S. R. *Adv. Mater.* **2011**, *23*, 268.
(21) Tang, C. W. *Appl. Phys. Lett.* **1986**, *48*, 183.
(22) Anthony, J. E. *Chem. Mater.* **2010**, *23*, 583.
(23) Chen, Z.; Lohr, A.; Saha-Möller, C. R.; Würthner, F. *Chem. Soc. Rev.* **2009**, *38*, 564.
(24) Rajaram, S.; Armstrong, P. B.; Kim, B. J.; Fréchet, J. M. J. *Chem. Mater.* **2009**, *21*, 1775.
(25) Markov, D. E.; Amsterdam, E.; Blom, P. W. M.; Sieval, A. B.; Hummelen, J. C. *J. Phys. Chem. A* **2005**, *109*, 5266.
(26) Shaw, P. E.; Ruseckas, A.; Samuel, I. D. W. *Adv. Mater.* **2008**, *20*, 3516.
(27) Schubert, A.; Settels, V.; Liu, W.; Würthner, F.; Meier, C.; Fink, R. F.; Schindlbeck, S.; Lochbrunner, S.; Engels, B.; Engel, V. *J. Phys. Chem. Lett.* **2013**, *4*, 792.
(28) Rajaram, S.; Shivanna, R.; Kandappa, S. K.; Narayan, K. S. *J. Phys. Chem. Lett.* **2012**, *3*, 2405.
(29) Sharenko, A.; Proctor, C. M.; van der Poll, T. S.; Henson, Z. B.; Nguyen, T.-Q.; Bazan, G. C. *Adv. Mater.* **2013**, *25*, 4403.
(30) Jiang, W.; Ye, L.; Li, X.; Xiao, C.; Tan, F.; Zhao, W.; Hou, J.; Wang, Z. *Chem. Commun.* **2014**, *50*, 1024.

(31) Lu, Z.; Jiang, B.; Zhang, X.; Tang, A.; Chen, L.; Zhan, C.; Yao, J. *Chem. Mater.* **2014**, *26*, 2907.

(32) Zhang, X.; Lu, Z.; Ye, L.; Zhan, C.; Hou, J.; Zhang, S.; Jiang, B.; Zhao, Y.; Huang, J.; Zhang, S.; Liu, Y.; Shi, Q.; Liu, Y.; Yao, J. *Adv. Mater.* **2013**, *25*, 5791.

(33) Shivanna, R.; Shoaee, S.; Dimitrov, S.; Kandappa, S. K.; Rajaram, S.; Durrant, J. R.; Narayan, K. S. *Energy Environ. Sci.* **2014**, *7*, 435.

(34) Zang, Y.; Li, C.-Z.; Chueh, C.-C.; Williams, S. T.; Jiang, W.; Wang, Z.-H.; Yu, J.-S.; Jen, A. K. Y. *Adv. Mater.* **2014**, *26*, 5708.

(35) Li, J.; Dierschke, F.; Wu, J.; Grimsdale, A. C.; Müllen, K. *J. Mater. Chem.* **2006**, *16*, 96.

(36) Hodgkiss, J. M.; Campbell, A. R.; Marsh, R. A.; Rao, A.; Albert-Seifried, S.; Friend, R. H. *Phys. Rev. Lett.* **2010**, *104*, 177701.

(37) McNeill, C. R.; Westenhoff, S.; Groves, C.; Friend, R. H.; Greenham, N. C. *J. Phys. Chem. C* **2007**, *111*, 19153.

(38) Gómez, R.; Veldman, D.; Blanco, R.; Seoane, C.; Segura, J. L.; Janssen, R. A. *Macromolecules* **2007**, *40*, 2760.

(39) Huang, C.; Potscavage, W. J.; Tiwari, S. P.; Sutcu, S.; Barlow, S.; Kippelen, B.; Marder, S. R. *Polym. Chem.* **2012**, *3*, 2996.

(40) Huang, J.; Wu, Y.; Fu, H.; Zhan, X.; Yao, J.; Barlow, S.; Marder, S. R. *J. Phys. Chem. A* **2009**, *113*, 5039.

(41) Sommer, M.; Lindner, S. M.; Thelakkat, M. *Adv. Funct. Mater.* **2007**, *17*, 1493.

(42) Sommer, M.; Lang, A. S.; Thelakkat, M. *Angew. Chem., Int. Ed.* **2008**, *47*, 7901.

(43) Marciniak, H.; Li, X.-Q.; Würthner, F.; Lochbrunner, S. *J. Phys. Chem. A* **2010**, *115*, 648.

(44) Margulies, E. A.; Shoer, L. E.; Eaton, S. W.; Wasielewski, M. R. *Phys. Chem. Chem. Phys.* **2014**, *16*, 23735.

(45) Eaton, S. W.; Shoer, L. E.; Karlen, S. D.; Dyar, S. M.; Margulies, E. A.; Veldkamp, B. S.; Ramanan, C.; Hartzler, D. A.; Savikhin, S.; Marks, T. J.; Wasielewski, M. R. *J. Am. Chem. Soc.* **2013**, *135*, 14701.

(46) Nakazono, S.; Easwaramoorthi, S.; Kim, D.; Shinokubo, H.; Osuka, A. *Org. Lett.* **2009**, *11*, 5426.

(47) Nakazono, S.; Imazaki, Y.; Yoo, H.; Yang, J.; Sasamori, T.; Tokitoh, N.; Cédric, T.; Kageyama, H.; Kim, D.; Shinokubo, H.; Osuka, A. *Chem.—Eur. J.* **2009**, *15*, 7530.

(48) Klebe, G.; Graser, F.; Hädicke, E.; Berndt, J. *Acta Crystallogr., Sect. B* **1989**, *45*, 69.

(49) Kazmaier, P. M.; Hoffmann, R. *J. Am. Chem. Soc.* **1994**, *116*, 9684.

(50) The dedicated high-resolution grazing-incidence X-ray scattering beamline 8-ID-E at the Advanced Photon Source.

(51) Lilliu, S.; Agostinelli, T.; Pires, E.; Hampton, M.; Nelson, J.; Macdonald, J. E. *Macromolecules* **2011**, *44*, 2725.

(52) Smilgies, D.-M. *J. Appl. Crystallogr.* **2009**, *42*, 1030.

(53) Giaimo, J. M.; Lockard, J. V.; Sinks, L. E.; Scott, A. M.; Wilson, T. M.; Wasielewski, M. R. *J. Phys. Chem. A* **2008**, *112*, 2322.

(54) Kamm, V.; Battagliarin, G.; Howard, I. A.; Pisula, W.; Mavrinskiy, A.; Li, C.; Müllen, K.; Laquai, F. *Adv. Energy Mater.* **2011**, *1*, 297.

(55) Zang, L.; Che, Y.; Moore, J. S. *Acc. Chem. Res.* **2008**, *41*, 1596.

(56) Settels, V.; Liu, W.; Pflaum, J.; Fink, R. F.; Engels, B. *J. Comput. Chem.* **2012**, *33*, 1544.

(57) Fink, R. F.; Seibt, J.; Engel, V.; Renz, M.; Kaupp, M.; Lochbrunner, S.; Zhao, H.-M.; Pfister, J.; Würthner, F.; Engels, B. *J. Am. Chem. Soc.* **2008**, *130*, 12858.

(58) Lou, S. J.; Szarko, J. M.; Xu, T.; Yu, L.; Marks, T. J.; Chen, L. X. *J. Am. Chem. Soc.* **2011**, *133*, 20661.

(59) Sharenko, A.; Gehrig, D.; Laquai, F.; Nguyen, T.-Q. *Chem. Mater.* **2014**, *26*, 4109−4118.

(60) Li, G.; Nitzan, A.; Ratner, M. A. *Phys. Chem. Chem. Phys.* **2012**, *14*, 14270.

(61) Scharber, M. C.; Mühlbacher, D.; Koppe, M.; Denk, P.; Waldauf, C.; Heeger, A. J.; Brabec, C. J. *Adv. Mater.* **2006**, *18*, 789.

(62) Servaites, J. D.; Ratner, M. A.; Marks, T. J. *Energy Environ. Sci.* **2011**, *4*, 4410.

(63) Mauer, R.; Howard, I. A.; Laquai, F. *J. Phys. Chem. Lett.* **2010**, *1*, 3500.

(64) Vandewal, K.; Tvingstedt, K.; Gadisa, A.; Inganas, O.; Manca, J. V. *Nat. Mater.* **2009**, *8*, 904.

(65) Lin, Y.; Zhan, X. *Mater. Horiz.* **2014**, *1*, 470.

(66) Mihailetchi, V. D.; Xie, H. X.; de Boer, B.; Koster, L. J. A.; Blom, P. W. M. *Adv. Funct. Mater.* **2006**, *16*, 699.

(67) Li, G.; Zhu, R.; Yang, Y. *Nat. Photonics* **2012**, *6*, 153.

(68) Sylvester-Hvid, K. O. *J. Phys. Chem. B* **2006**, *110*, 2618.

(69) Szarko, J. M.; Guo, J.; Liang, Y.; Lee, B.; Rolczynski, B. S.; Strzalka, J.; Xu, T.; Loser, S.; Marks, T. J.; Yu, L. *Adv. Mater.* **2010**, *22*, 5468.

(70) Facchetti, A. *Mater. Today* **2013**, *16*, 123.

(71) Bakulin, A. A.; Rao, A.; Pavelyev, V. G.; van Loosdrecht, P. H.; Pshenichnikov, M. S.; Niedzialek, D.; Cornil, J.; Beljonne, D.; Friend, R. H. *Science* **2012**, *335*, 1340.

(72) Rybtchinski, B.; Sinks, L. E.; Wasielewski, M. R. *J. Phys. Chem. A* **2004**, *108*, 7497.

(73) van der Boom, T.; Hayes, R. T.; Zhao, Y.; Bushard, P. J.; Weiss, E. A.; Wasielewski, M. R. *J. Am. Chem. Soc.* **2002**, *124*, 9582.

(74) Gosztola, D.; Niemczyk, M. P.; Svec, W.; Lukas, A. S.; Wasielewski, M. R. *J. Phys. Chem. A* **2000**, *104*, 6545.

(75) Holcombe, T. W.; Norton, J. E.; Rivnay, J.; Woo, C. H.; Goris, L.; Piliego, C.; Griffini, G.; Sellinger, A.; Brédas, J.-L.; Salleo, A.; Fréchet, J. M. J. *J. Am. Chem. Soc.* **2011**, *133*, 12106.

(76) Pensack, R. D.; Guo, C.; Vakhshouri, K.; Gomez, E. D.; Asbury, J. B. *J. Phys. Chem. C* **2012**, *116*, 4824.

(77) Jailaubekov, A. E.; Willard, A. P.; Tritsch, J. R.; Chan, W.-L.; Sai, N.; Gearba, R.; Kaake, L. G.; Williams, K. J.; Leung, K.; Rossky, P. J.; Zhu, X. Y. *Nat. Mater.* **2013**, *12*, 66.